

Comparison of Spectral and Wavelet Estimators of Transfer Function for Linear Systems

M. A. A. Bakar^{1,2,*}, D. A. Green² and A. V. Metcalfe²

¹ School of Mathematical Sciences, Faculty of Science and Technology, Universiti Kebangsaan Malaysia, UKM Bangi, Selangor, Malaysia.

² School of Mathematical Sciences, University of Adelaide, South Australia, Australia.

Received 17 May 2012; Accepted (in revised version) 27 July 2012

Available online 23 August 2012

Abstract. We compare spectral and wavelet estimators of the response amplitude operator (RAO) of a linear system, with various input signals and added noise scenarios. The comparison is based on a model of a heaving buoy wave energy device (HBWED), which oscillates vertically as a single mode of vibration linear system. HBWEDs and other single degree of freedom wave energy devices such as oscillating wave surge converters (OWSC) are currently deployed in the ocean, making such devices important systems to both model and analyse in some detail. The results of the comparison relate to any linear system. It was found that the wavelet estimator of the RAO offers no advantage over the spectral estimators if both input and response time series data are noise free and long time series are available. If there is noise on only the response time series, only the wavelet estimator or the spectral estimator that uses the cross-spectrum of the input and response signals in the numerator should be used. For the case of noise on only the input time series, only the spectral estimator that uses the cross-spectrum in the denominator gives a sensible estimate of the RAO. If both the input and response signals are corrupted with noise, a modification to both the input and response spectrum estimates can provide a good estimator of the RAO. A combination of wavelet and spectral methods is introduced as an alternative RAO estimator. The conclusions apply for autoregressive emulators of sea surface elevation, impulse, and pseudorandom binary sequences (PRBS) inputs. However, a wavelet estimator is needed in the special case of a chirp input where the signal has a continuously varying frequency.

AMS subject classifications: 65M10, 78A48

Key words: Heaving buoy, spectral analysis, discrete wavelet transform, impulse response, response amplitude operator.

*Corresponding author. Email address: aftar@ukm.my (M. A. A. Bakar)

1. Introduction

Several studies have promoted the wavelet transform (WT) as an alternative to spectral analysis (SA) for estimating the response amplitude operator (RAO) of linear systems [15, 29, 30]. The study of these systems is important because all structures are sensitive to vibration and some exploit this vibration. A stable linear system will respond to a stationary sinusoidal input at some specific frequency by vibrating at that frequency. However, the amplitude of the response relative to the amplitude of the input, known as the RAO or gain, depends on the frequency. There is also a phase shift, which depends on the frequency. Given this characterisation of a linear system, it is often more convenient to study the linear system in the frequency domain instead of in the time domain. Wavelet transforms have a potential advantage of displaying frequency composition over time. In contrast, the definition of a population spectrum as the Fourier transform of the autocovariance function is based on the assumption of a stationary random process.

The use of spectral analysis to estimate the RAO is justified for a general input rather than a stationary input, if the spectrum is considered as a sample estimate of a Fourier transform. A blow from an impact hammer, an accessory for spectrum analysers commonly used in model testing for lightweight structures, is a good example of a non-stationary input. Since spectral estimation of the RAO is not limited to a stationary input, it follows that the WT may not necessarily offer any advantage over the SA.

In this paper, we compare WT methods with SA methods for estimating the RAO of a linear system, with different classes of input signals and with different distributions of noise corrupting either input or response signals. The comparison is set in the context of a wave tank model of a heaving buoy wave energy device (HBWED). The reasons for this choice are that wave energy devices generally are receiving renewed attention as the need for renewable energy resources becomes increasingly apparent, and their response to the random wave environment is crucial for design. Specifically, the HBWED can plausibly be modelled as a single mode of the vibration system, and this allows a straightforward comparison of WT and SA estimation of the RAO. The oscillating wave surge converters (OWSC) are single degree of freedom devices — but the OWSC oscillates horizontally in surge instead of oscillating vertically in heave as the HBWED, and is nonlinear [32].

Spectral analysis has been used in the study of dynamic systems for many decades (e.g. see [14]), and the spectrum analyser has been standard equipment in test laboratories since the 1960s [13]. In contrast, although the Haar sequence was proposed in 1909 [10], the mathematical generalisation and the use of WT for the analysis of dynamic systems is still in the development stage [15, 21, 24]. Since a wavelet is localised in the time-scale domain, certain information can be accessed directly and immediately from the wavelet representation of a time series. This multiscale feature of wavelet transforms can be used to validate a dynamic model from a continuous wavelet transform of the process observations and model time series data [21].

Wavelets enable the detection of even very weak signals by using local amplification and compression, which has been advantageous in analysing dynamic systems. By using a wavelet transform, the random property of a chaotic response can also be observed

— even for very short time series data such as in [33], where the authors have applied wavelet transform techniques to analyse the nonlinear dynamic system of ship roll and heave-roll coupling. Pernot & Lamarque [26] have computed the transient responses of parametrically excited dynamic systems by using wavelet transforms and also used them for a stability analysis of linear systems. Gouttebroze [9] used a wavelet identification technique to identify the characteristics of structural systems, by analysing the amplitude and phase of a wavelet transform for vibration data. Other applications of wavelets include solving differential equations, turbulence analysis, image processing and signal processing [11].

2. Case Study

A heaving buoy wave energy device (HBWED) has been selected as the case study for the comparison. The HBWED is a deep water wave energy device that has reached the stage of commercial development. An HBWED called PowerBuoy (cf. Fig. 1) developed by Ocean Power Technologies Inc. has been deployed at the northeast coast of Scotland, and is soon to be deployed along the southwest coast of Victoria, Australia [25]. The study of the dynamic system that models the HBWED provides a basis for an investigation of issues affecting wave energy development, such as efficiency and engineering design. For example, Masubuchi *et al.* [19] have analysed the frequency response of an ocean wave energy device with two floating bodies. The dynamic behaviour of the system can be understood from that study, and hence the energy absorption from ocean waves can be optimised.

2.1. Heaving buoy with one degree of freedom

A heaving buoy wave energy device such as in Fig. 1 is constrained to move in the vertical (heave) direction only, so the motion of this device can be modelled as a linear dynamic system with a single mode of vibration [28]. A mathematical description for this device is a second order differential equation of the form

$$\ddot{y} + 2\zeta\omega_n\dot{y} + \omega_n^2y = u, \quad (2.1)$$

where ζ is the damping factor, ω_n is the undamped natural frequency and $\sqrt{\omega_n^2(1-\zeta^2)}$ is the damped natural frequency of the system.

In this investigation, we adopt $\zeta = 0.2$ and $\omega_n = 0.05$ as realistic values for a wave tank model of a HBWED. Thus Eq. (2.1) can be written as

$$\ddot{y} + 0.02\dot{y} + 0.0025y = u. \quad (2.2)$$

The solution can be expressed as a convolution integral

$$y(t) = \int_{-\infty}^t h(t-\tau)u(\tau)d\tau, \quad (2.3)$$



Figure 1: Deployed heaving buoy device PowerBuoy, at the northeast coast of Scotland. [25]

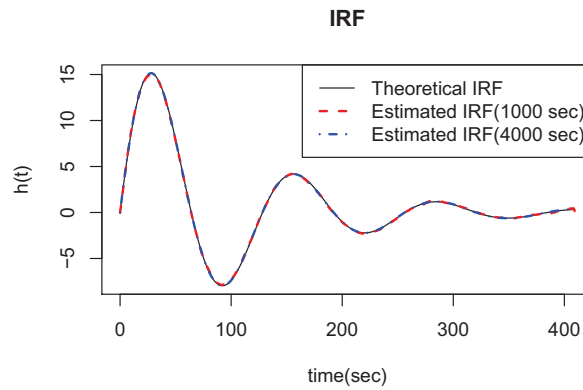


Figure 2: Theoretical IRF and wavelet estimates of the IRF (without noise).

where $h(t)$ is the impulse response function (IRF) of the linear system. The response to a unit impulse for the system given in Eq. (2.1) is

$$h(t) = \frac{1}{\omega_n \sqrt{1 - \zeta^2}} e^{-\zeta \omega_n t} \sin\left(\sqrt{1 - \zeta^2} \omega_n t\right). \quad (2.4)$$

For our particular case Eq. (2.2), the impulse response function (IRF) is given by

$$h(t) = \frac{1}{0.05 \sqrt{0.96}} e^{-0.01t} \sin\left(0.05 \sqrt{0.96} t\right), \quad (2.5)$$

which is plotted in Fig. 2. The undamped natural frequency of the system described by Eq. (2.2) is $\omega_n = 0.05$ rad/sec and the natural frequency is $\sqrt{\omega_n^2 (1 - \zeta^2)} \approx 0.049$ rad/sec. The Fourier transform of the convolution product in Eq. (2.3) used below is

$$Y(\omega) = H(\omega) \cdot U(\omega), \quad (2.6)$$

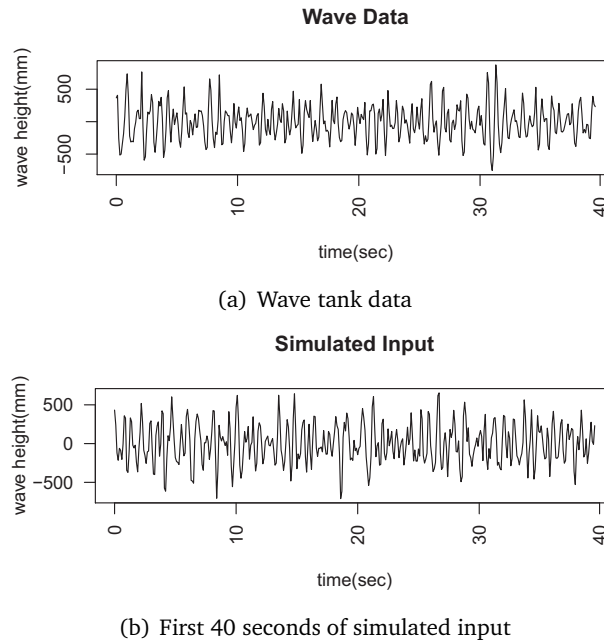


Figure 3: Wave tank data and first 40 seconds of simulated time series input.

where $Y(\omega)$, $H(\omega)$ and $U(\omega)$ denote the Fourier transforms of $y(t)$, $h(t)$ and $u(t)$ respectively.

2.2. Input based on wave tank data

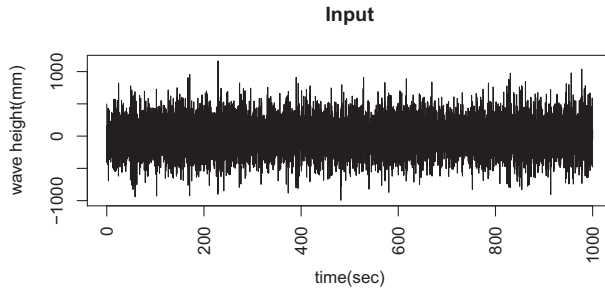
A time series of wave tank data $\{u_t; t = 1, 2, \dots, 396\}$ sampled at 0.1 second intervals [12] is shown in Fig. 3(a). This time series is too short for our investigation, but was adopted to determine the coefficients for an autoregressive model $AR(p)$ to simulate stationary time series input — e.g. see [3].

The most suitable autoregressive model, based on the Akaike information criterion (AIC) [1] and consideration of the residuals, is an $AR(13)$ given by

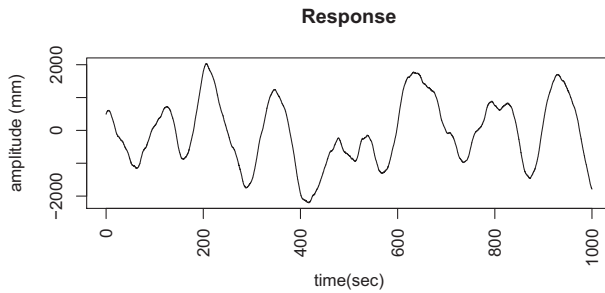
$$\begin{aligned}
 u_t = & 0.4016u_{t-1} - 0.8701u_{t-2} - 0.2660u_{t-3} - 0.5223u_{t-4} - 0.5154u_{t-5} \\
 & - 0.5076u_{t-6} - 0.3935u_{t-7} - 0.3831u_{t-8} - 0.2614u_{t-9} - 0.3748u_{t-10} \\
 & - 0.0866u_{t-11} - 0.1398u_{t-12} - 0.0735u_{t-13} + w_t, \quad (2.7)
 \end{aligned}$$

where w_t is a Gaussian (Normal) variate with mean 0 and standard deviation 149.3. A realisation of length 40,000 from the $AR(13)$ model, corresponding to 4,000 seconds sampled every 0.1 second, was initially used as the input to the model of the HBWED. The first 1,000 seconds of input are shown in Fig. 4(a) and the first 40 seconds are shown in Fig. 3(b), which is qualitatively similar to the original time series in Fig. 3(a).

The digitised input data is denoted as $\{u_t\}$, while $\{y_t\}$ is the digitised response. From Eq. (2.1), the response at time t can be approximated by a difference equation. Using



(a) First 1000 seconds of input



(b) First 1000 seconds of response

Figure 4: Input and response time series.

central differences, the approximation for the first derivative is of the form

$$\dot{y}_t \approx \frac{y_{t+1} - y_{t-1}}{2\Delta}, \tag{2.8}$$

and for the second derivative of form

$$\ddot{y}_t \approx \frac{y_{t+1} - 2y_t + y_{t-1}}{\Delta^2} \tag{2.9}$$

where Δ is the sampling interval [20]. Thus an approximation of the response for the linear system in Eq. (2.1) is given by

$$y_t = a_1 y_{t-1} + a_2 y_{t-2} + a_0 u_{t-1}, \tag{2.10}$$

where

$$a_0 = \frac{\Delta^2}{1 + \zeta \omega_n \Delta}, \quad a_1 = \frac{2 - \omega_n^2 \Delta^2}{1 + \zeta \omega_n \Delta}, \quad a_2 = \frac{\zeta \omega_n \Delta - 1}{1 + \zeta \omega_n \Delta}.$$

With $\Delta = 0.1$ sec, an approximation of the response for the specific system in Eq. (2.1) is therefore

$$y_t = \frac{1.99975}{1.00100} y_{t-1} - \frac{0.999}{1.001} y_{t-2} + \frac{0.010}{1.001} u_{t-1}, \tag{2.11}$$

which is plotted in Fig. 4(b) over 1,000 seconds.

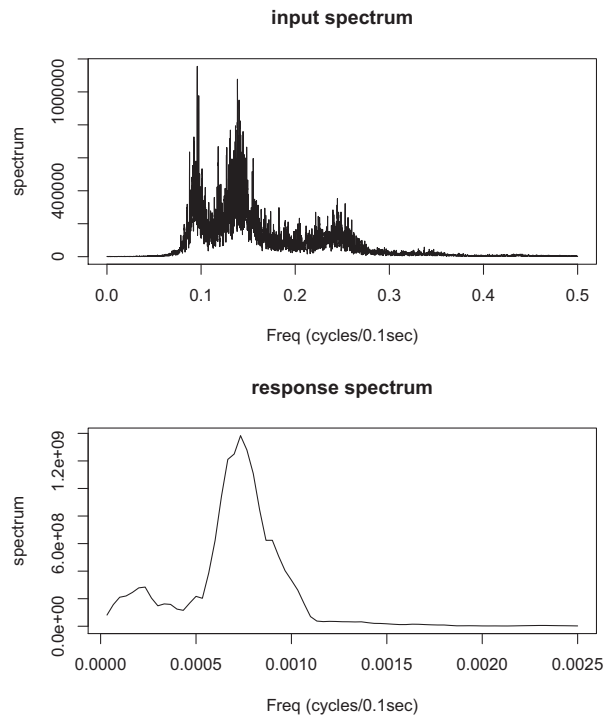


Figure 5: Input and response spectra.

3. Estimation of Transfer Function

The frequency composition of a stationary stochastic process is described by its spectrum, which is defined as the Fourier transform of its autocovariance function [4]. This spectrum can be estimated by smoothing the sample periodogram [12]. If the sample time series is of length N , then the periodogram has spikes at $N/2$ specific frequencies from $2\pi/N\Delta$ up to π/Δ . However, these must be smoothed to produce consistent estimates of the true population spectrum. The number of spikes that are averaged is known as the span [6]. The span must be wide enough to remove spurious peaks, but not so wide that true peaks are substantially reduced. With short time series, these conflicting requirements lead to unreliable estimates of the spectrum. Another consideration is that the specific frequencies of the periodogram depend only on the length of the time series, and generally will not coincide with any deterministic frequency present in a non-stationary time series. The deterministic frequency will leak out into neighbouring spikes. Fig. 5 shows the spectra for the input and response time series used in this study, with a span of 16 and time series length 40,000.

A linear dynamic system can be characterised by its transfer function, which describes its response to disturbances at specific frequencies. In a marine context, the modulus of the transfer function is known as the response amplitude operator (RAO) [12], and in electrical engineering it is known as the gain. If the spectrum of the disturbance and the

RAO is known, then the spectrum for the response can be calculated. Alternatively, the RAO can be estimated as the ratio of the response sample spectrum to the input sample spectrum. The RAO characterises the response of marine structures that can plausibly be modelled as linear systems, such as a HBWED or cargo ships, to sea states [22]. Other applications of the RAO include the response of other vehicles such as cars on uneven road surfaces and aircraft on a runway. Another aspect of spectral analysis is that any sudden change in the spectrum of noise from a machine can be an early warning of a defect. Such monitoring is called signature analysis, and together with preventative maintenance can avoid catastrophic failure.

3.1. Spectral estimators

Let the input signal be given by

$$u_t = Ue^{i\omega t}, \quad (3.1)$$

where U is a real number representing the amplitude of the input. Similarly, let the response be given by

$$y_t = Ye^{i(\omega t + \phi)}, \quad (3.2)$$

where Y is a real number representing the amplitude of the response and ϕ is the phase shift given by the linear system. By substituting Eqs. (3.1) and (3.2) into the second order differential equation of the linear dynamical system Eq. (2.1), we see that

$$-\omega^2 Ye^{i(\omega t + \phi)} + i2\zeta\omega_n Y\omega e^{i(\omega t + \phi)} + \omega_n^2 Ye^{i(\omega t + \phi)} = Ue^{i\omega t}. \quad (3.3)$$

Eq. (3.3) leads to

$$\frac{Y}{U} = \frac{e^{-i\phi}}{\omega_n^2 - \omega^2 + i2\zeta\omega_n\omega}, \quad (3.4)$$

and the RAO or gain is given by

$$G(\omega) = \left| \frac{e^{-i\phi}}{\omega_n^2 - \omega^2 + i2\zeta\omega_n\omega} \right| = \frac{1}{\sqrt{(\omega_n^2 - \omega^2)^2 + 4\zeta^2\omega_n^2\omega^2}}. \quad (3.5)$$

This is the same as $H(\omega)$ in Eq. (2.6), a fact that is used with the wavelet estimator of the RAO. The maximum value for the RAO is

$$G_{\max} = 1 / \left(\zeta\omega_n^2 \sqrt{4 - 3\zeta^2} \right), \quad (3.6)$$

when the frequency is equal to $\sqrt{\omega_n^2(1 - \zeta^2)}$. Furthermore, the phase shift is

$$\phi = \tan^{-1} \left(-\frac{2\zeta\omega_n\omega}{\omega_n^2 - \omega^2} \right). \quad (3.7)$$

For a linear system with single input u_t and single response y_t , the RAO can be estimated by

$$|\widehat{G}_2(\omega)| = \sqrt{\frac{C_{yy}}{C_{uu}}}, \quad (3.8)$$

where C_{uu} and C_{yy} are the sample spectra of the input and response respectively. However, this estimator is sensitive to noise. An alternative estimator, which is unaffected by noise on the response, is the ratio of the cross-spectrum of the input and the response to the spectrum of the input — i.e.

$$\widehat{G}_1(\omega) = \frac{|C_{uy}|}{C_{uu}}, \quad (3.9)$$

where C_{uy} is the sample cross-spectrum of the input and response. The cross-spectrum is the Fourier Transform of the cross-covariance function of the input and response time series — e.g. see [12]. Similarly, the estimator

$$\widehat{G}_3(\omega) = \frac{C_{yy}}{|C_{yu}|} \quad (3.10)$$

is unaffected by noise on the input [2].

A related statistic is the coherence, defined as

$$\widehat{\text{coh}}(\omega) = \frac{|C_{uy}|^2}{C_{uu}C_{yy}} = \frac{\widehat{G}_1^2}{\widehat{G}_2^2}. \quad (3.11)$$

The coherence can be thought of as the square of the correlation coefficient between the input and response over frequency, and its value is therefore between 0 and 1. It can be used to detect noise on input, noise on response, nonlinearity, compensated delays and leakage (resolution bias) in the linear system.

If there is noise on both the input and the response, one strategy is to use \widehat{G}_2 , after making an allowance for the noise component in the computed C_{uu} and C_{yy} . The allowance considered here is to assume the high frequency component of the computed C_{uu} and C_{yy} is due to noise, and that the noise is white and has a flat spectrum. Computationally, this modification is implemented as a subtraction of the average of the spectrum ordinates over the highest 1/20 of the frequency range from all the spectrum ordinates. This modification of \widehat{G}_2 is denoted by

$$|\widehat{G}_4(\omega)| = \sqrt{\frac{C_{yy}^-}{C_{uu}^-}}, \quad (3.12)$$

where C_{uu}^- and C_{yy}^- are the modified spectrum estimates.

3.2. Wavelet IRF estimator

Wavelet transforms are defined in continuous and discrete forms. In statistical studies, sample data are usually taken in discrete form, so we only discuss the discrete wavelet transform (DWT).

The DWT of a signal of length n yields the DWT coefficients, consisting of $J - 1$ levels of wavelet coefficients $\{W_{j,k}\}$ and $J - 1$ levels of scaling coefficients $\{V_{j,k}\}$, where $j = 0, \dots, J - 1$, $J = \log_2(n)$, $k = 0, \dots, N_j - 1$ and $N_j = 2^j$. A simpler and faster technique to perform the discrete wavelet transform, known as the DWT pyramid algorithm, was introduced by Mallat [18]. By using the DWT pyramid algorithm, the coefficients can be calculated by

$$W_{j,k} = \sum_{l=0}^{L-1} \psi_l V_{j+1,2k+1-l \bmod N_{j+1}}, \tag{3.13}$$

$$V_{j,k} = \sum_{l=0}^{L-1} \varphi_l V_{j+1,2k+1-l \bmod N_{j+1}}, \tag{3.14}$$

where ψ is the wavelet filter, φ is the scaling filter, L is the width of the filter and $V_{j,k} = x_k$, with $\{x_k; k = 0, 1, 2, \dots, n - 1\}$ the time series data. In this analysis, the Haar wavelet is used where

$$\psi_l^{\text{Haar}} = \begin{cases} -1/\sqrt{2} & l = 0 \\ 1/\sqrt{2} & l = 1 \end{cases}, \tag{3.15}$$

$$\varphi_l^{\text{Haar}} = \begin{cases} 1/\sqrt{2} & l = 0 \\ 1/\sqrt{2} & l = 1 \end{cases}. \tag{3.16}$$

Consider a time series $\{x_t; t = 1, 2, 3, \dots, n\}$. The DWT of $\{x_t\}$ can be represented by the sequence

$$\mathbf{x}^{\text{DWT}} = [\tilde{x}_1 \quad \tilde{x}_2 \quad \tilde{x}_3 \quad \tilde{x}_4 \quad \dots \quad \tilde{x}_n], \tag{3.17}$$

where $\tilde{x}_1 = V_{0,0}$ is the vector of scaling coefficients at level 0, $\tilde{x}_2 = W_{0,0}$ is the vector of wavelet coefficients at level 0, $\tilde{x}_3 = W_{1,0}$ and $\tilde{x}_4 = W_{1,1}$ are the first and second wavelet coefficients at level 1, and $\tilde{x}_n = W_{J-1,N_{j-1}-1}$ are the final wavelet coefficients at level $J - 1$.

An interesting feature of the wavelet transform is that the signal can be recovered from its wavelet and scaling coefficients by the inverse discrete wavelet transform (IDWT). It can be performed by using Mallat's pyramid algorithm defined as

$$V_{j,k} = \sum_{l=0}^{L-1} \psi_l W_{j-1,k+l \bmod N_j}^\uparrow + \sum_{l=0}^{L-1} \varphi_l V_{j-1,k+l \bmod N_j}^\uparrow, \tag{3.18}$$

where

$$W_{j,k}^\uparrow = \begin{cases} 0 & k = 0, 2, \dots, N_{j+1} \\ W_{j, \frac{k-1}{2}} & k = 1, 3, \dots, N_{j+1} - 1 \end{cases}, \tag{3.19}$$

$$V_{j,k}^\uparrow = \begin{cases} 0 & k = 0, 2, \dots, N_{j+1} \\ V_{j, \frac{k-1}{2}} & k = 1, 3, \dots, N_{j+1} - 1 \end{cases}. \tag{3.20}$$

Following Newland [24],

$$y_n = \Delta \mathbf{h}^{\text{DWT}} \cdot \mathbf{u}^{\text{DWT}}, \tag{3.21}$$

where

$$\mathbf{h}^{\text{DWT}} = \begin{bmatrix} \tilde{h}_1 & \tilde{h}_2 & \tilde{h}_3 & \tilde{h}_4 & \cdots & \tilde{h}_n \end{bmatrix},$$

$$\mathbf{u}^{\text{DWT}} = \begin{bmatrix} \tilde{u}_1 \\ \tilde{u}_2 \\ \tilde{u}_3/2 \\ \tilde{u}_4/2 \\ \tilde{u}_5/4 \\ \vdots \\ \tilde{u}_n/2^{J-1} \end{bmatrix}.$$

Here \mathbf{h}^{DWT} is the DWT of the IRF, \mathbf{u}^{DWT} is the DWT of the input time series $\{\mathbf{u}_{n-\theta}, 1 \leq \theta \leq n\}$, y_n is the response at time n and Δ is the sampling interval. For $N - n + 1$ responses, Eq. (3.21) can be written in matrix form

$$\mathbf{Y} = \Delta \mathbf{h}^{\text{DWT}} \cdot \mathbf{U}^{\text{DWT}}, \quad (3.22)$$

where

$$\mathbf{Y} = \begin{bmatrix} y_n & y_{n+1} & \cdots & y_N \end{bmatrix},$$

$$\mathbf{h}^{\text{DWT}} = \begin{bmatrix} \tilde{h}_1 & \tilde{h}_2 & \cdots & \tilde{h}_n \end{bmatrix},$$

$$\mathbf{U}^{\text{DWT}} = \begin{bmatrix} \mathbf{u}_n^{\text{DWT}} & \mathbf{u}_{n+1}^{\text{DWT}} & \cdots & \mathbf{u}_N^{\text{DWT}} \end{bmatrix},$$

and $\mathbf{u}_i^{\text{DWT}}$ is the DWT of $\{\mathbf{u}_{i-\theta}, 1 \leq \theta \leq n\}$. If the number of inputs is $N = 64$ and $n = 16$, the number of responses that can be calculated by equation 3.22 is $N - n + 1 = 49$. Thus Eq. (3.22) can be rewritten as

$$[y_{16} \ y_{17} \ \cdots \ y_{64}] = \Delta \begin{bmatrix} \tilde{h}_1 & \tilde{h}_2 & \cdots & \tilde{h}_{16} \end{bmatrix}$$

$$\times \begin{bmatrix} \tilde{u}_1^{(16)} & \tilde{u}_1^{(17)} & \cdots & \tilde{u}_1^{(64)} \\ \tilde{u}_2^{(16)} & \tilde{u}_2^{(17)} & \cdots & \tilde{u}_2^{(64)} \\ \tilde{u}_3^{(16)}/2 & \tilde{u}_3^{(17)}/2 & \cdots & \tilde{u}_3^{(64)}/2 \\ \tilde{u}_4^{(16)}/2 & \tilde{u}_4^{(17)}/2 & \cdots & \tilde{u}_4^{(64)}/2 \\ \tilde{u}_5^{(16)}/4 & \tilde{u}_5^{(17)}/4 & \cdots & \tilde{u}_5^{(64)}/4 \\ \vdots & \vdots & \ddots & \vdots \\ \tilde{u}_{16}^{(16)}/8 & \tilde{u}_{16}^{(17)}/8 & \cdots & \tilde{u}_{16}^{(64)}/8 \end{bmatrix}. \quad (3.23)$$

Robertson *et al.* [29] propose a method to estimate the IRF when the inputs and responses of a linear dynamic system are known, using the above relation. From Eq. (3.22), the DWT of the IRF can be estimated by

$$\mathbf{h}^{\text{DWT}} = \frac{1}{\Delta} \mathbf{Y} \cdot \mathbf{U}^{\text{DWT}^T} \cdot \left(\mathbf{U}^{\text{DWT}} \cdot \mathbf{U}^{\text{DWT}^T} \right)^{-1}. \quad (3.24)$$

Thus the IRF can be found by the inverse DWT of the terms $\mathbf{h}^{\text{DWT}}/2^J$ — i.e.

$$\{h_i, i = 1, 2, \dots, n\} = \text{IDWT} \{ \mathbf{h}^{\text{DWT}}/2^J \}, \quad (3.25)$$

where $J = \log_2 n$. However, this operation cannot be directly implemented if we use the wavelet packages in MATLAB or in R software [27]. Some alteration should be made to Eq. (3.21-3.25), so that this wavelet estimation of the RAO can be used without producing any error.

From Eq. (3.21), the factor $1/2^j$ is removed from the DWT coefficients of input time series such as

$$\mathbf{u}^{\text{DWT}^T} = [\tilde{u}_1 \quad \tilde{u}_2 \quad \tilde{u}_3 \quad \tilde{u}_4 \quad \dots \quad \tilde{u}_n] . \quad (3.26)$$

Thus the matrix operation shown in Eq. (3.23) becomes

$$\begin{aligned} [y_{16} \quad y_{17} \quad \dots \quad y_{64}] &= \Delta [\tilde{h}_1 \quad \tilde{h}_2 \quad \dots \quad \tilde{h}_{16}] \\ &\times \begin{bmatrix} \tilde{u}_1^{(16)} & \tilde{u}_1^{(17)} & \dots & \tilde{u}_1^{(64)} \\ \tilde{u}_2^{(16)} & \tilde{u}_2^{(17)} & \dots & \tilde{u}_2^{(64)} \\ \tilde{u}_3^{(16)} & \tilde{u}_3^{(17)} & \dots & \tilde{u}_3^{(64)} \\ \vdots & \vdots & \ddots & \vdots \\ \tilde{u}_{16}^{(16)} & \tilde{u}_{16}^{(17)} & \dots & \tilde{u}_{16}^{(64)} \end{bmatrix} . \end{aligned} \quad (3.27)$$

It is notable that the first $n - 1$ response values are lost from the previous matrix operation. However, this can be overcome by introducing $n - 1$ zeroes before the first input time series so that the input time series record length becomes $N + n - 1$, where the first $n - 1$ values are zero — i.e. $\{u_1^{\text{new}} = 0, u_2^{\text{new}} = 0, \dots, u_{n-1}^{\text{new}} = 0, u_n^{\text{new}} = u_1, u_{n+1}^{\text{new}} = u_2, \dots, u_{N-n+1}^{\text{new}} = u_N\}$. This is because there is essentially a zero signal prior to time 0. Thus from Eq. (3.22), for N responses

$$\mathbf{Y} = \Delta \mathbf{h}^{\text{DWT}} \cdot \hat{\mathbf{U}}^{\text{DWT}}, \quad (3.28)$$

where

$$\begin{aligned} \mathbf{Y} &= [y_1 \quad y_2 \quad \dots \quad y_N] , \\ \mathbf{h}^{\text{DWT}} &= [\tilde{h}_1 \quad \tilde{h}_2 \quad \dots \quad \tilde{h}_n] , \\ \hat{\mathbf{U}}^{\text{DWT}} &= [\hat{\mathbf{u}}_n^{\text{DWT}} \quad \hat{\mathbf{u}}_{n+1}^{\text{DWT}} \quad \dots \quad \hat{\mathbf{u}}_{N+n-1}^{\text{DWT}}] , \end{aligned}$$

and $\hat{\mathbf{u}}_i^{\text{DWT}}$ is the DWT of $\{u_{i-\theta}^{\text{new}}, 1 \leq \theta \leq n\}$. Consequently, Eq. (3.27) can be rewritten as

$$\begin{aligned} [y_1 \quad y_2 \quad \dots \quad y_{64}] &= \Delta [\tilde{h}_1 \quad \tilde{h}_2 \quad \dots \quad \tilde{h}_{16}] \\ &\times \begin{bmatrix} \tilde{u}_1^{(16)} & \tilde{u}_1^{(17)} & \dots & \tilde{u}_1^{(79)} \\ \tilde{u}_2^{(16)} & \tilde{u}_2^{(17)} & \dots & \tilde{u}_2^{(79)} \\ \tilde{u}_3^{(16)} & \tilde{u}_3^{(17)} & \dots & \tilde{u}_3^{(79)} \\ \vdots & \vdots & \ddots & \vdots \\ \tilde{u}_{16}^{(16)} & \tilde{u}_{16}^{(17)} & \dots & \tilde{u}_{16}^{(79)} \end{bmatrix} . \end{aligned} \quad (3.29)$$

To find the DWT of the IRF, we use the same step as in Eq. (3.24). However, to find the IRF we do not need to divide the DWT of the IRF by 2^J as in Eq. (3.25) — i.e. we use

$$\{h_i, i = 1, 2, \dots, n\} = \text{IDWT} \{ \mathbf{h}^{\text{DWT}} \}, \quad (3.30)$$

where $J = \log_2 n$. From the discrete Fourier Transform, the wavelet-estimated IRF can give us the wavelet-estimated RAO as

$$\widehat{G}_w(\omega_t) = \Delta |H(\omega_t)| = \Delta \left| \sum_{k=1}^n h_k e^{-i2\pi \frac{t}{n} k} \right|, \quad (3.31)$$

where $H(\omega_t)$ is the discrete Fourier Transform of the wavelet-estimated IRF involving $\omega_t = t/(n\Delta)$ and $t = 1, \dots, n$.

3.3. Multiple regression IRF estimator

Alternatively, we can use multiple regression to estimate the discretised impulse response $\{h_i, i = 1, 2, \dots, n\}$, defined as

$$y_t = h_1 u_t + h_2 u_{t-1} + \dots + h_n u_{t-n} + \epsilon_t, \quad (3.32)$$

where $t = n - 1, \dots, N$ and ϵ_t is the discrete white noise. In matrix form, Eq. (3.32) can be written as

$$\mathbf{Y} = \mathbf{h} \cdot \mathbf{U} + \boldsymbol{\epsilon}. \quad (3.33)$$

The IRF h_i can be estimated by the least squares method

$$\mathbf{h} = \frac{1}{\Delta} \mathbf{Y} \cdot \mathbf{U}^T \cdot (\mathbf{U} \cdot \mathbf{U}^T)^{-1}. \quad (3.34)$$

However, multiple regression provided in the R software [27] uses a lot of computational memory for storage overhead, especially if we use long time series data.

3.4. Combined wavelet-spectral method

Both the wavelet and spectral analysis discussed give good estimates of the RAO for data without noise. If there is noise on the response time series, \widehat{G}_1 and \widehat{G}_w give good estimates of the RAO provided the noise is not correlated with the input signal. Meanwhile, \widehat{G}_3 is a good RAO estimator if there is noise on the input time series, and \widehat{G}_4 can be used if there is noise on both input and response signals. However, wavelet analysis can also offer another alternative RAO estimator if there is noise on the input time series only, or if there is noise on both input and response time series. If the noise is intermittent, wavelet analysis can be used to select noise-free sub-series, from which the RAO can be estimated by spectral methods. If the noise is stationary and independent, and the input signal is relatively low frequency, the standard deviation of the noise σ_w can be estimated as the mean absolute deviation (MAD) of the finest scale wavelet coefficients [8]. In this context,

the MAD — computed in R with the `mad()` function [23] — is the median of the absolute values of deviations from the median [27].

The estimate of the RAO is

$$|\widehat{G}_{ws}(\omega)| = \sqrt{\frac{C_{yy}}{C_{\widehat{uu}} - C_{ww}}} \quad (3.35)$$

where $C_{\widehat{uu}}$ is the estimated spectrum of the noisy measurement of the input and C_{ww} is the spectrum of the noise. If we assume the noise is white, then the estimate of C_{ww} is $\hat{\sigma}_w^2/0.05$.

4. Estimates of the Transfer Function of a Heaving Buoy

4.1. No noise

For this investigation, the AR(13) input and the response time series discussed in Section 2.2 were used to estimate the IRF for the linear dynamical system of Eq. (2.1). Two lengths of time series were considered, to compare each method dependency with the time series length. The shorter time series was of length $T = 1000$ seconds, and the longer time series was $T = 4000$ seconds. Initially, the Haar wavelet (the simplest type of wavelet filter) was selected for the analysis. The wavelet estimate of the IRF for length $T = 1000$ seconds and $T = 4000$ seconds are plotted in Fig. 2, which shows a very similar value between those two cases and also with the theoretical IRF. The Fourier transform of the IRF is the estimate of the RAO.

To make the comparison, the wavelet and spectral estimates of the RAO are plotted with the theoretical RAO in Fig. 6 for both cases. For spectral estimates, the span values were set at 4 and 16 for the shorter and longer time series respectively, to smooth the estimates of the RAO and prevent identifying spurious peaks. In Fig. 6(a), we see that the spectral estimates based on the shorter time series with span 4 underestimate the peak at the natural frequency, but \widehat{G}_3 is less biased than \widehat{G}_2 and \widehat{G}_1 . The wavelet estimate is the least biased. The bandwidth of the spectral estimation is $\frac{S}{0.5/(N/2)}$ Hz, where S is the span and N is the time series length. The coherence function is relatively low around the natural frequency, reflecting the difference between \widehat{G}_1 and \widehat{G}_2 . With the longer time series, the span was set to 16 but the number of spikes in the spectra were increased by a factor of 4 and the resulting bandwidth was narrower. For this longer time series, all four estimates shown in Fig. 6(b) are close to the theoretical value. We therefore conclude that the time series length of the input and the response data play an important role in estimating the RAO via the spectral methods. The data with longer time series (4,000 sec and hence 40,000 data) was needed to obtain a reliable estimate of the RAO.

In the previous analysis, the Haar wavelet was used in the wavelet method. To show that this method works for other types of wavelet, the Daubechies D(4) [7] wavelet has also been used. Fig. 7 shows that the difference between the wavelet estimate of the RAO using the Daubechies D(4) wavelet and the wavelet estimate of the RAO using the

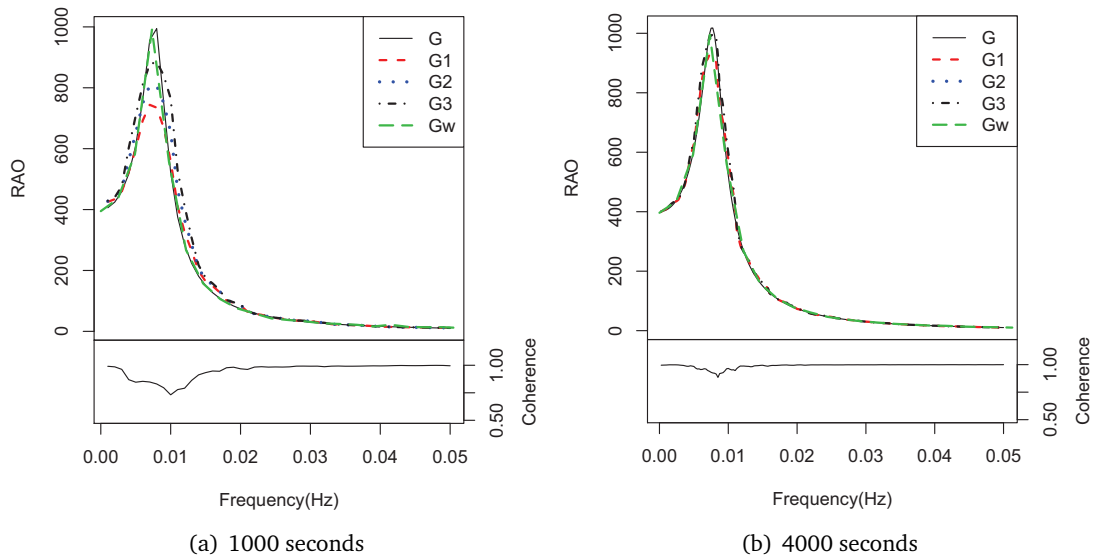


Figure 6: Coherence and the comparison of spectral and wavelet estimates of RAO (without noise).

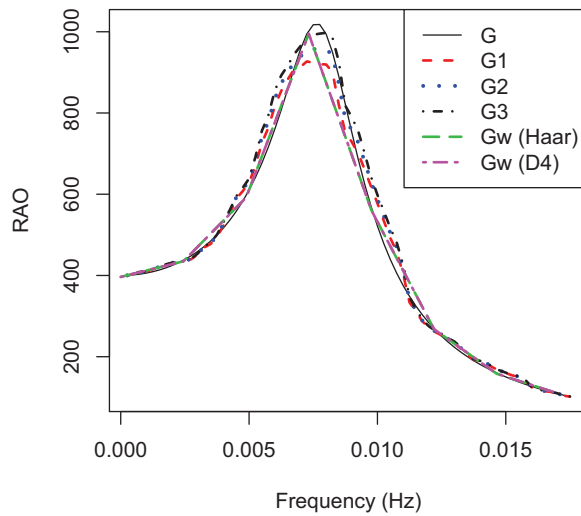


Figure 7: Peak of the theoretical RAO and comparison of spectral and wavelet estimates of RAO (Haar and D4 wavelet, without noise).

Haar wavelet is imperceptible. Thus even when the simpler (Haar) wavelet was used, the wavelet method gave a good estimate of the RAO.

4.2. Noise on the response

Two types of noise were considered for the case of noise on the response time series — viz.

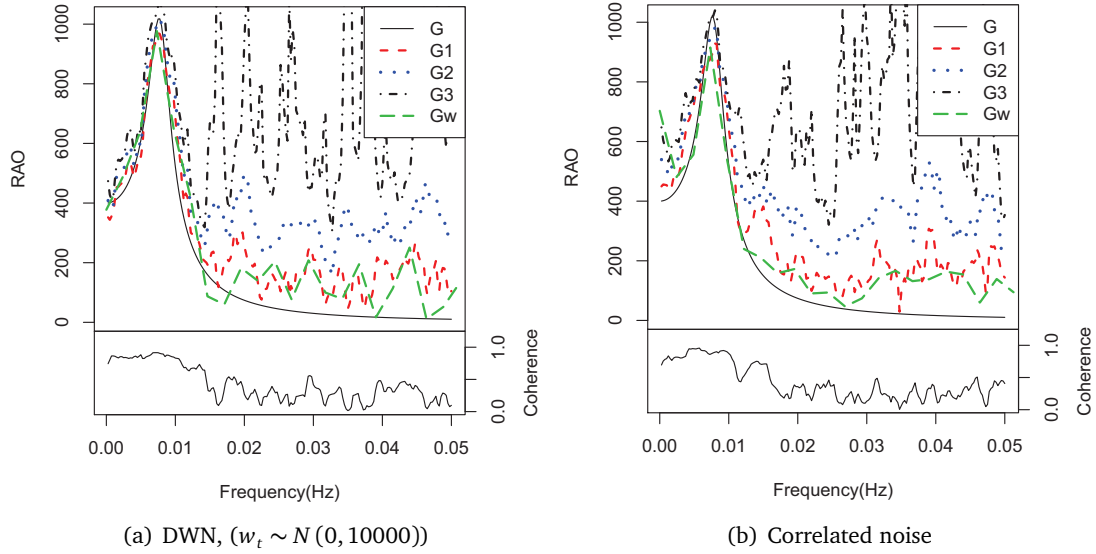


Figure 8: Coherence and the comparison of spectral and wavelet estimates of RAO (noise on the response).

1. discrete white noise (DWN), w_t is a Gaussian with mean 0 and standard deviation 10000,
2. correlated noise, $n_t = 0.9n_{t-1} + w_t$ where w_t is a Gaussian with mean 0 and standard deviation 1000.

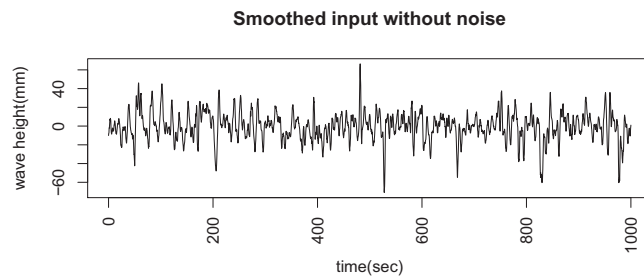
From Fig. 8(a) it can be seen that \widehat{G}_1 and \widehat{G}_w are less affected by the noise than \widehat{G}_2 , while \widehat{G}_3 is worse. Both \widehat{G}_1 and \widehat{G}_w are very similar at the peak, but \widehat{G}_w is less affected by the noise at higher frequencies. The coherence is relatively low at high frequencies, which is to be expected because the response of the system to high frequency forcing is slight and the noise dominates. All the estimates are poor as the frequency tends to 0. The results with correlated noise are qualitatively similar. The \widehat{G}_1 is insensitive to noise uncorrelated with the input because this noise does not affect the cross-covariance of the input and response signal. The wavelet estimator is insensitive to noise, since the wavelet method is equivalent to fitting the regression model

$$y_t = \beta_0 + \beta_1 u_t + \beta_2 u_{t-1} + \cdots + n_t \quad (4.1)$$

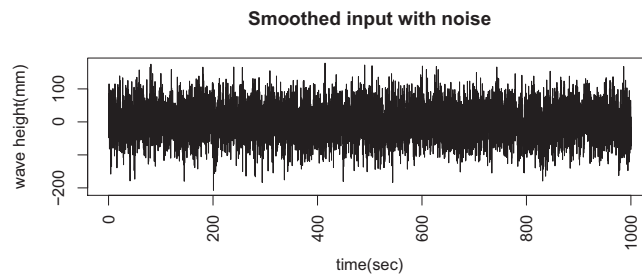
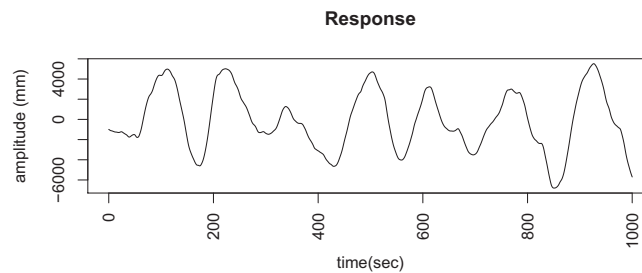
by ordinary least squares. The noise n_t added to the response does not bias the estimates $\hat{\beta}_0, \hat{\beta}_1, \dots$ and $\hat{\beta}_n$, even if it is autocorrelated.

4.3. Noise on the input

To demonstrate the method of Section 3.4, we smooth the autoregressive input by taking a locally weighted scatterplot smoothing (LOESS) method. The smoothed input and response time series are shown in Fig. 9, and the DWT coefficients of this smoothed



(a) First 1000 seconds of smoothed input without noise

(b) First 1000 seconds of smoothed input with noise, $v_t \sim N(0, 50)$ 

(c) First 1000 seconds of response

Figure 9: Smoothed input and response time series.

input are shown in Fig. 10(a). Gaussian white noise with mean 0 and standard deviation 50.0 was added to the smoothed input, and the DWT coefficients of this noise-corrupted measurement of the input are shown in Fig. 10(b). The estimate of the standard deviation of the noise is 49.7. It is shown in Fig. 11(a) that \widehat{G}_{ws} is as good as \widehat{G}_3 when the noise on the input signal is discrete white noise, because from Eq. (3.35) the noise spectrum has been removed from the input. However, other estimators of the RAO are affected by the added noise on the input time series.

The correlated noise $n_t = 0.9n_{t-1} + v_t$ was also considered, where v_t is Gaussian with mean 0 and standard deviation 10. However, the combined wavelet-spectral estimate \widehat{G}_{ws} of the RAO is not as good as the spectral estimator \widehat{G}_3 because the correlated noise spectrum is not flat, unlike the discrete white noise spectrum.

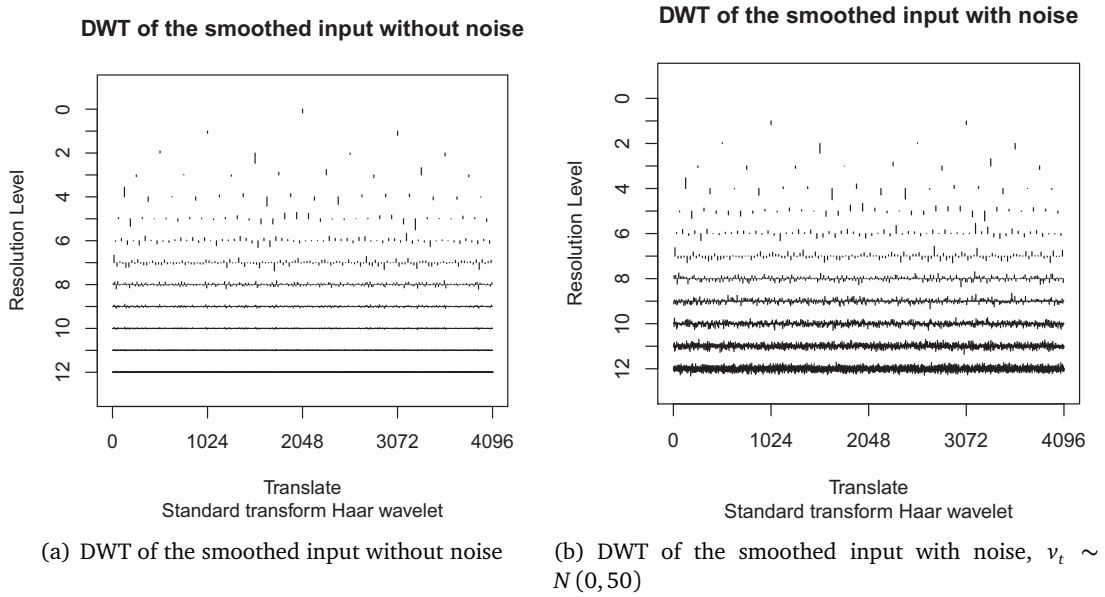


Figure 10: Plot of the DWT coefficients.

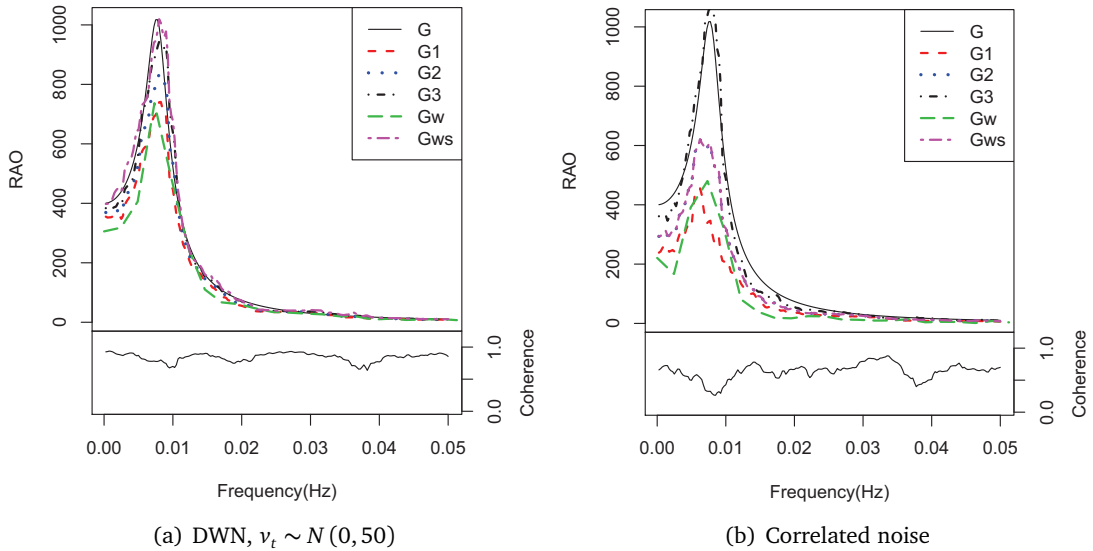


Figure 11: Coherence and the comparison of spectral, wavelet and combined wavelet-spectral estimates of RAO (noise on the input).

4.4. Noise on both the input and the response

Noise on both the input and the response time series was also considered, where the added noise is discrete white noise. In Fig. 12, the modified spectral estimate \hat{G}_4 is seen to be better than other estimators. This is to be expected, since \hat{G}_4 uses the modified input

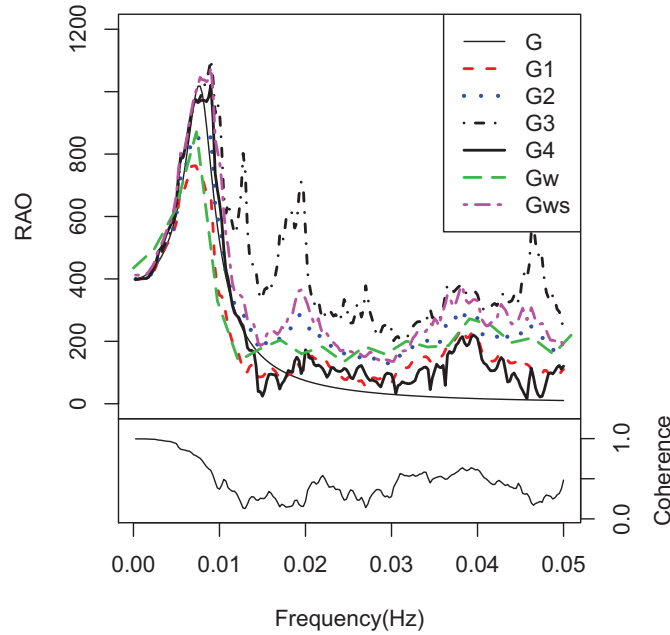


Figure 12: Coherence and the comparison of spectral, wavelet and combined wavelet-spectral estimates of RAO (DWN noise on the input, $v_t \sim N(0, 50)$, and on the response, $w_t \sim N(0, 20000)$).

and response spectrum estimates. The combined wavelet-spectral estimate \hat{G}_{ws} gives a good estimate of the RAO's peak, but gets worse at higher frequency.

4.5. Different types of input signals

Four different types of signal were also considered as the input to the single mode of vibration linear system in Eq. (2.2) — viz.

1. chirp signal with constant amplitude,
2. chirp signal with increasing amplitude,
3. unit impulse signal,
4. pseudorandom binary sequence (PRBS) signal.

The responses are shown in Fig. 13.

Comparisons of both spectral and wavelet RAO estimators are shown in Fig. 14. For both of the chirp input signal cases, it is seen that the spectral methods are not suitable to estimate the RAO, whereas the wavelet method performs very well. For the PRBS and the unit impulse signal, the wavelet estimator is only marginally better than the spectral estimators on the peak of the RAO. Differences are caused by the selected bandwidth/span of the spectral analysis package, which over-smoothed the spectrum estimation and hence biased the RAO spectral estimates, especially at the peak response.

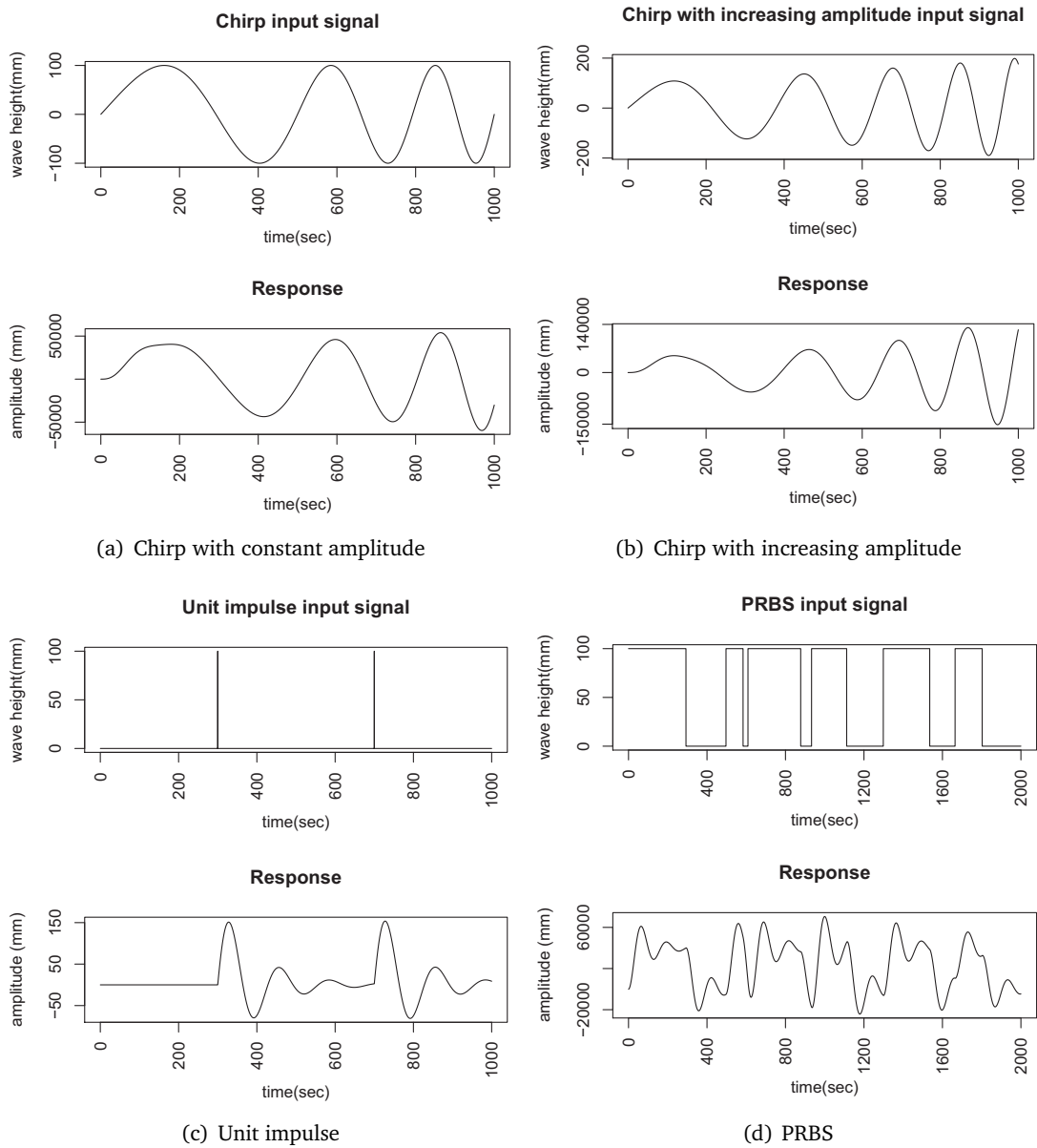


Figure 13: Input and response time series for different types of input signals.

5. Conclusions and Discussions

Spectral analysis is a well established technique for estimating the RAO of linear systems. With long data records such as might be gathered over 1 hour at a sampling rate of 10 per second, and negligible signal noise, \widehat{G}_w offers no significant advantage over \widehat{G}_1 , \widehat{G}_2 or \widehat{G}_3 — and the detail around the peak is worse (cf. Fig. 7). The poor detail around

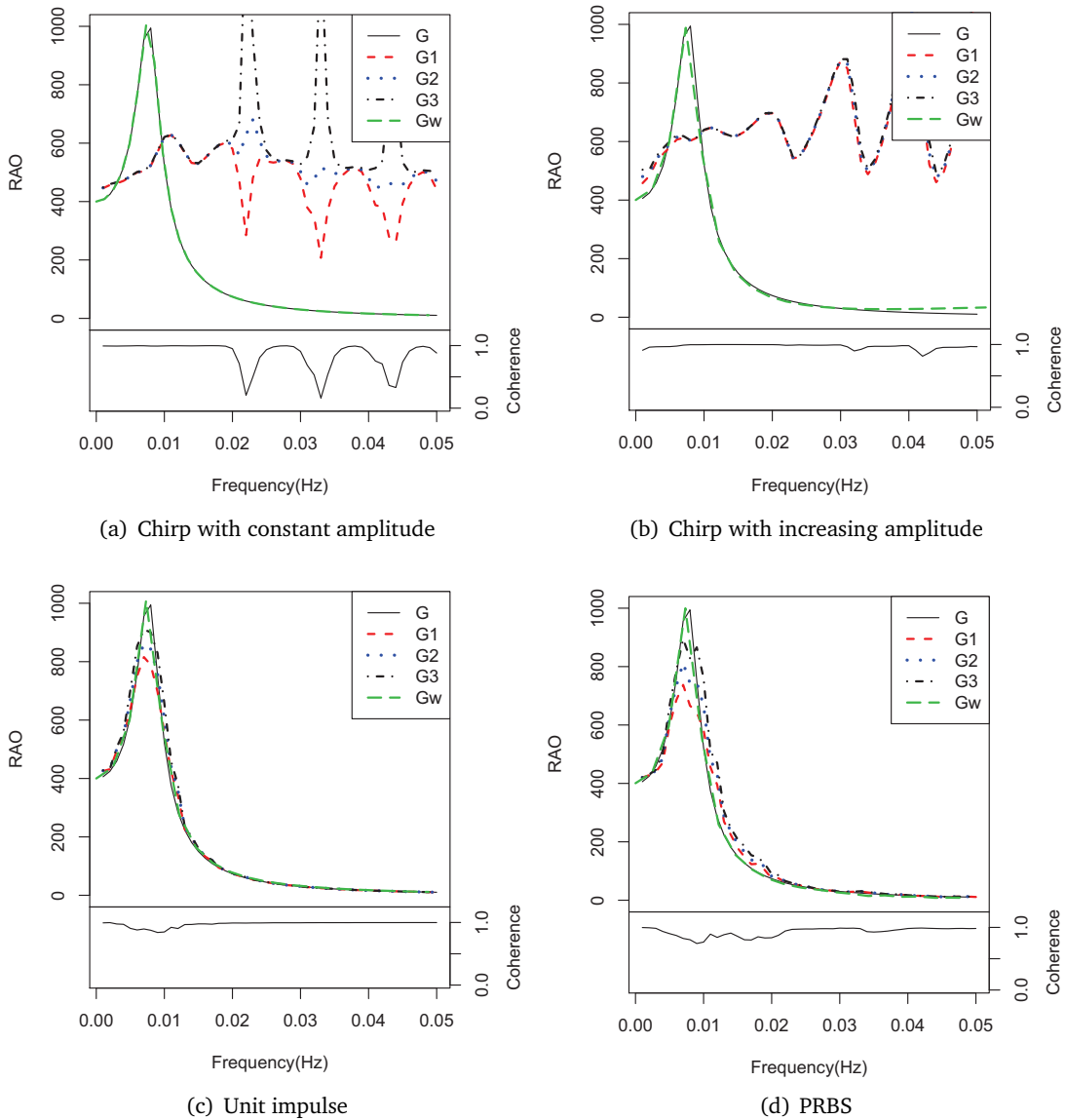


Figure 14: Coherence and the comparison of spectral and wavelet estimates of RAO for different types of input signals

the peak is due to the relatively small number of points in the estimate of the impulse response, because of limits on the sizes of the non-sparse matrices that can be inverted.

For shorter records consisting of a few thousand data, \widehat{G}_w is better at identifying the magnitude of the peak response (Fig. 6(a)). The estimation of an RAO from a short time series of a few hundred points, such as might arise in economics, requires considerable smoothing of estimated spectra by autoregressive estimators, or of the IRF. We have made no comparisons, as in most RAO estimation it is possible to obtain long time series, typically

sampled from some analogue measuring device.

If there is only noise on the response, \widehat{G}_1 should be used rather than \widehat{G}_2 , and \widehat{G}_3 should not be used. Theoretically, both \widehat{G}_w and \widehat{G}_1 are not biased by noise that is independent of the input, although the precision of the estimate will be reduced. However, when there is noise only on the input \widehat{G}_3 gives a very good estimate of the RAO compared to \widehat{G}_1 , \widehat{G}_2 and \widehat{G}_w . Noise on both the input and response time series affects all three spectral estimators (\widehat{G}_1 , \widehat{G}_2 and \widehat{G}_3), and the wavelet estimator (\widehat{G}_w) of the RAO. However, by using \widehat{G}_4 we can still get a good estimate of the RAO by making some modifications to the computed spectra. A combination of the wavelet transform to either identify noise free periods or to estimate the variance of the noise and hence modify the input spectrum, followed by SA, also shows promise.

In Section 4.5, it was shown that the SA is inappropriate if the input signal has a continuously varying frequency, such as for chirp signals. In contrast, the wavelet method is able to deal with such special cases.

\widehat{G}_w relies on estimation of the IRF, from which the RAO is estimated by taking its Fourier transform. The IRF can also be estimated directly without recourse to the wavelet transform, by fitting a multiple regression model using ordinary least squares (OLS). For a given number of points in the IRF, the matrix to be inverted has the same eigenvalues as that for the wavelet method, and neither matrix is sparse. For our case study, the condition number was 11.78 for OLS and 10.45 for wavelets. When using R software [27], we were surprised that the computation time was nearly double with OLS. However, OLS has the advantage that the time series does not have to be dyadic (have a length that is a power of 2). The choice between using wavelets or OLS to estimate the IRF will typically depend on the available software.

The theory and estimation of RAO depends on the assumed linear dynamics, but it yields a reasonable approximation for many dynamical systems. However, there is considerable scope for the application of wavelets in nonlinear dynamics, and it is now an active research area [5, 16, 17, 31]. This application of wavelets, especially to the single mode of a vibration system, could be beneficial for the development of nonlinear single degree of freedom wave energy devices such as the OWSC and variants of HBWED.

Acknowledgments

The authors acknowledge the developer of the open source software R [27], and express deep appreciation to the Universiti Kebangsaan Malaysia and the Ministry of Higher Education Malaysia for the financial allocation for this work.

Notation

u_t	input time series
y_t	response time series
ζ	damping factor
ω_n	undamped natural frequency

Δ	sampling interval
h_t	impulse response
$U(\omega), Y(\omega), H(\omega)$	Fourier transform of u_t, y_t, h_t
U, Y	absolute value of $U(\omega), Y(\omega)$
C_{uu}	input spectrum
C_{yy}	response spectrum
C_{uy}	input-response cross-spectrum
$G(\omega)$	theoretical RAO
$\widehat{G}_1(\omega), \widehat{G}_2(\omega), \widehat{G}_3(\omega)$	spectral RAO estimators
$\widehat{G}_4(\omega)$	modified spectral RAO estimator
$\widehat{\text{coh}}(\omega)$	coherence
$W_{j,k}$	wavelet coefficients
$V_{j,k}$	scaling coefficients
ψ	wavelet filter
ϕ	scaling filter
\mathbf{x}^{DWT}	DWT of $\{x_t\}$
$\widehat{G}_w(\omega)$	wavelet RAO estimator
$\widehat{G}_{ws}(\omega)$	combined wavelet-spectral RAO estimator
v_t and w_t	white noise on the input and response time series
n_t	correlated noise time series

References

- [1] H. Akaike. A new look at the statistical model identification. *Automatic Control, IEEE Transactions on*, 19(6):716–723, 1974.
- [2] J. S. Bendat and A. G. Piersol. *Random Data: Analysis and Measurement Procedures*, volume 729. Wiley, 2011.
- [3] G. E. P. Box, G. M. Jenkins, and G. C. Reinsel. *Time Series Analysis*. Holden-day San Francisco, 1976.
- [4] R. N. Bracewell. *The Fourier Transform & Its Applications* 3rd Ed. McGraw-Hill, 2000.
- [5] S. L. Chen, J. J. Liu, and H. C. Lai. Wavelet analysis for identification of damping ratios and natural frequencies. *Journal of Sound and Vibration*, 323(1-2):130–147, 2009.
- [6] P. S. P. Cowpertwait, A. Metcalfe, and A. V. Metcalfe. *Introductory Time Series with R*. Springer Verlag, 2009.
- [7] I. Daubechies. *Ten Lectures on Wavelets*, volume 61. Society for Industrial Mathematics, 1992.
- [8] D. L. Donoho and I. M. Johnstone. Ideal spatial adaptation by wavelet shrinkage. *Biometrika*, 81(3):425–455, 1994.
- [9] S. Gouttebroze and J. Lardies. On using the wavelet transform in modal analysis. *Mechanics Research Communications*, 28(5):561–569, 2001.
- [10] A. Haar. Zur theorie der orthogonalen funktionensysteme. *Mathematische Annalen*, 69(3):331–371, 1910.
- [11] W. Hardle, G. Kerkycharian, D. Picard, and A. Tsybakov. *Wavelets, Approximation and Statistical Applications*. Springer-Verlag, New York, 1998.
- [12] G. E. Hearn and A. Metcalfe. *Spectral Analysis in Engineering: Concepts and Cases*. Arnold, London, 1995.

- [13] W. R. Hewlett. *Inventions of Opportunity: Matching Technology With Market Needs*. Hewlett Packard Co, 1983.
- [14] G.M. Jenkins and D.G. Watts. *Spectral Analysis and Its Applications*. Holden-Day, 1968.
- [15] Y. Y. Kim, J. C. Hong, and N. Y. Lee. Frequency response function estimation via a robust wavelet de-noising method. *Journal of Sound and Vibration*, 244(4):635 – 649, 2001.
- [16] Y. Kitada. Identification of nonlinear structural dynamic systems using wavelets. *Journal of Engineering Mechanics*, 124(10):1059, 1998.
- [17] D. T. L. Lee and A. Yamamoto. Wavelet analysis: Theory and applications. *Hewlett-Packard Journal*, 45:44 – 54, 1994.
- [18] S. Mallat. *A Wavelet Tour of Signal Processing*. Academic Press, 1999.
- [19] M. Masubuchi and R. Kawatani. Frequency response analysis of an ocean wave energy converter. *Journal of Dynamic Systems, Measurement, and Control*, 105(1):30–38, 1983.
- [20] J. H. Mathews and K. D. Fink. *Numerical Methods Using MATLAB*, volume 31. Prentice Hall Upper Saddle River, 1999.
- [21] J. R. McCusker, K. Danai, and D. O. Kazmer. Validation of dynamic models in the time-scale domain. *Journal of Dynamic Systems, Measurement, and Control*, 132(6):061402, 2010.
- [22] A. Metcalfe, L. Maurits, T. Svenson, R. Thach, and G. E. Hearn. Modal analysis of a small ship sea keeping trial. *Australian & New Zealand Industrial and Applied Mathematics Journal*, 47:915–933, July 2007.
- [23] G. P. Nason. *Wavelet Methods in Statistics with R*. Springer-Verlag, New York, 2008.
- [24] D. E. Newland. *An Introduction to Random Vibrations, Spectral and Wavelet Analysis*. Longman Scientific & Technical, 1993.
- [25] Ocean Power Technologies, Inc. *Making Waves in Power*. <http://www.oceanpowertechnologies.com>.
- [26] S. Pernot and C. H. Lamarque. A wavelet-galerkin procedure to investigate time-periodic systems: Transient vibration and stability analysis. *Journal of Sound and Vibration*, 245(5):845–875, 2001.
- [27] R Development Core Team. *R: A Language and Environment for Statistical Computing*. R Foundation for Statistical Computing, Vienna, Austria, 2008.
- [28] J. Ringwood. The dynamics of wave energy. In *Proceeding of Irish Signal and Systems Conference*, June 2006.
- [29] A. N. Robertson, K. C. Park, and K. F. Alvin. Extraction of impulse response data via wavelet transform for structural system identification. *Journal of Vibration and Acoustics*, 120(1):252–260, 1998.
- [30] A. N. Robertson, K. C. Park, and K. F. Alvin. Identification of structural dynamics models using wavelet-generated impulse response data. *Journal of Vibration and Acoustics*, 120(1):261–266, 1998.
- [31] W. J. Staszewski. Analysis of non-linear systems using wavelets. *Proceedings of the Institution of Mechanical Engineers – Part C, Journal of Mechanical Engineering Science*, 214(11):1339 – 1353, 2000.
- [32] T. Whittaker and M. Folley. Nearshore oscillating wave surge converters and the development of oyster. *Philosophical Transactions of The Royal Society A*, 370:345–364, 2012.
- [33] Y. Yu, R. Ajit Sheno, H. Zhu, and L. Xia. Using wavelet transforms to analyze nonlinear ship rolling and heave-roll coupling. *Ocean Engineering*, 33(7):912–926, 2006.